SUPPORTING INFORMATION

Multi-colour uranyl emission efficiently tuned by hexacyanidometallates within hybrid coordination frameworks

Szymon Chorazy,* Jakub J. Zakrzewski, Mateusz Reczyński and Barbara Sieklucka

Faculty of Chemistry, Jagiellonian University, Gronostajowa 2, 30-387 Krakow, Poland.

*Corresponding author: chorazy@chemia.uj.edu.pl

Experimental details

Materials

Uranyl nitrate hexahydrate, $UO_2(NO_3)_2 \cdot 6H_2O$ (99%), containing depleted uranium, was purchased from BDH Chemicals. Potassium hexacyanidoplatinate(IV), $K_2[Pt(CN)_6]$ (99.9%) and potassium hexacyanidocobaltate(III), $K_3[Co(CN)_6]$ (97%) were received from Sigma-Aldrich. Potassium hexacyanidoiridate(III), $K_3[Ir(CN)_6]$ (99%) was purchased from abcr GmbH. Potassium hexacyanidorhodate(III), $K_3[Rh(CN)_6]$ was prepared according to previously published synthetic procedure,[S1] using rhodium(III) chloride hydrate, $RhCl_3 \cdot xH_2O$ (99.9%, Sigma-Aldrich). The organic ligand, 4,4'-bipyridyl-N,N'-dioxide (4,4'-bpdo) was prepared according to previously published synthetic procedure,[S2] using 4,4'-bipyridine (98%, Alfa Aesar) as a starting material. All precursors obtained from commercial sources were used without additional purification.

[S1] (*a*) M. C. Read, J. Glaser, I. Person and M. Sandström, *J. Chem. Soc., Dalton Trans.*, 1994, 3243; (*b*) J. Wang, S. Chorazy, K. Nakabayashi, B. Sieklucka and S. Ohkoshi, *J. Mater. Chem. C*, 2018, **6**, 473.

[S2] G. M. Sequiera, W. Y. Tan, E. G. Moore, *Dalton Trans*. 2015, **44**, 13378.

Synthesis and basic characterization of 1–4

Synthesis of 1. The 60.3 mg (0.12 mmol) portion of $UO_2(NO_3)_2 \cdot 6H_2O$, and the 22.7 mg (0.12 mmol) portion of 4,4-bipyridyl-N,N'-dioxide (4,4'-bpdo) were dissolved together in 4 mL of distilled water. A water solution (2 mL) of the 40.0 mg (0.12 mmol) portion of $K_3[Co(CN)_6]$ was added which resulted in the formation of amorphous precipitate. After ca. one week the precipitate recrystallized entirely, forming needle-like yellow crystals of **1** which were collected by a suction filtration, washed by a small amount of distilled water and ethanol, and dried on the air. The composition of **1**, $[(UO_2)_2(OH)(4,4'\text{-bpdo})_2][Co(CN)_6] \cdot 0.5H_2O$, was identified by a single-crystal X-ray diffraction analysis. The crystals of **1** are stable on the air, preserving the composition and the crystal structure, as was proved by CHN elemental analysis, and powder X-ray diffraction analysis. Yield: 52.6 mg, 76%.

IR spectrum of **1** (Figure S1). Cyanides stretching vibrations: 2110 cm^{-1}, 2134 cm^{-1}, 2148 cm^{-1} and 2170 cm^{-1}. A series of peaks in the 1600-800 cm^{-1} range confirm the presence of 4,4'-bpdo ligand,[S3] while the broad range and complex pattern of IR peaks of cyanide stretching vibrations indicates the presence of both bridging and terminal cyanides within hexacyanidocobaltate(III) units.[S4] CHN elemental analysis. Anal. Calcd. for $U_4Co_2C_{52}H_{36}N_{20}O_{19}$ ($M_W = 2314.95$ g·mol^{-1}): C, 27.0%; H, 1.6%; N, 12.1%. Found: C, 27.3%; H, 1.9%; 12.4%.

Synthesis of 2. Compound **2** was obtained in the same manner as presented above for **1**, but using $K_3[Rh(CN)_6]$ instead of $K_3[Co(CN)_6]$. The amorphous precipitate left for recrystallization in the mother solution produced yellow needle crystals of **2** after two weeks. Their composition of $[(UO_2)_2(OH)(4,4'\text{-bpdo})_2][Rh(CN)_6] \cdot 0.1H_2O$ was determined by a single-crystal X-ray diffraction analysis. After drying on the air, the crystals of **2** absorb additional water molecules, as depicted by CHN elemental analysis, showing the composition of $[(UO_2)_2(OH)(4,4'\text{-bpdo})_2][Rh(CN)_6] \cdot 4.5H_2O$ (**2hyd**) for the air-stable phase. However, the sample of **2hyd** preserves the crystal structure of **2** which was confirmed by a powder X-ray diffraction analysis. Yield: 37.9 mg, 50%.

IR spectrum of **2** (Figure S1). Cyanides stretching vibrations: 2121 cm^{-1}, 2142 cm^{-1}, 2166 cm^{-1} and 2186 cm^{-1}. A series of peaks in the 1600-800 cm^{-1} range confirm the presence of 4,4'-bpdo ligand,[S3] while four peaks of the cyanide stretching vibrations represent the presence of both bridging and terminal cyanides in **2**.[S1b,S4] CHN elemental analysis. Anal. Calcd. for $U_4Rh_2C_{52}H_{52}N_{20}O_{27}$ (M_W = 2547.02 g·mol^{-1}): C, 24.5%; H, 2.1%; N, 11.0%. Found: C, 24.0%; H, 2.0%; 11.5%.

Synthesis of 3. The analogous synthetic procedure to those presented for **1** was used, with the exception of using $K_3[Ir(CN)_6]$ instead of $K_3[Co(CN)_6]$ precursor. The precipitate left for recrystallization in the mother solution gave yellow needle crystals of **3** after two weeks. Their composition of $[(UO_2)_2(OH)(4,4'\text{-bpdo})_2][Ir(CN)_6]\cdot 0.5H_2O$ was found within a single-crystal X-ray diffraction structural analysis. The crystals of **3** are stable on the air as confirmed by CHN elemental analysis, and a powder X-ray diffraction analysis. Yield: 48.8 mg, 63%.

IR spectrum of **3** (Figure S1). Cyanides stretching vibrations: 2120 cm^{-1}, 2143 cm^{-1}, 2163 cm^{-1} and 2190 cm^{-1}. A series of peaks in the 1600-800 cm^{-1} range indicate the presence of 4,4'-bpdo ligand.[S3] The complex pattern of IR peaks of cyanide stretching vibrations indicates the presence of both bridging and terminal cyanides within hexacyanidoiridate(III) units.[S4] CHN elemental analysis. Anal. Calcd. for $U_4Co_2C_{52}H_{36}N_{20}O_{19}$ (M_W = 2581.52 g·mol^{-1}): C, 24.2%; H, 1.4%; N, 10.9%. Found: C, 23.9%; H, 1.7%; 11.2%.

Synthesis of 4. The 30.4 (0.06 mmol) portion of $UO_2(NO_3)_2\cdot 6H_2O$ and the 11.4 mg (0.06 mmol) portion of 4,4'-bpdo were dissolved together in 4 mL of distilled water. Then, a water solution (2 mL) of the 25.9 mg (0.06 mmol) of $K_2[Pt(CN)_6]$ was added, the resulting clear solution was stirred for several minutes, and left open for crystallization. Yellow plate crystals of **4** appeared after ca. one week. They were collected by a suction filtration, washed by a small amount of distilled water and ethanol, and dried on the air. The composition of **4**, $[(UO_2)_2(OH)_2(4,4'\text{-bpdo})_2][Pt(CN)_6]\cdot H_2O$, was identified by a single-crystal X-ray diffraction analysis. The crystals of **4** are stable on the air as confirmed by CHN elemental analysis, and a powder X-ray diffraction analysis. Yield: 34.4 mg, 87%.

IR spectrum of **4** (Figure S1). Cyanides stretching vibrations: 2185 cm^{-1} and 2216 cm^{-1}. A series of peaks in the 1600-800 cm^{-1} range confirm the presence of 4,4'-bpdo ligand.[S3] Two complex bands in the range of cyanides stretching vibrations prove the presence of bridging and terminal cyanides within $[Pt(CN)_6]^{2-}$ moieties.[S5] CHN elemental analysis. Anal. Calcd. for $U_2PtC_{26}H_{20}N_{10}O_{11}$ (M_W = 1319.64 g·mol^{-1}): C, 23.7%; H, 1.5%; N, 10.6%. Found: C, 24.1%; H, 1.7%; 10.9%.

[S3] S. Chorazy, R. Podgajny, W. Nitek, M. Rams, S. Ohkoshi and B. Sieklucka, *Cryst. Growth Des.*, 2013, **13**, 3036.

[S4] (*a*) T. Shiga, A. Mishima, K. Sugimoto, H. Okawa, H. Oshio and M. Ohba, *Eur. J. Inorg. Chem.*, 2012, 2784; (*b*) K. Kumar, S. Chorazy, K. Nakabayashi, H. Sato, B. Sieklucka, S. Ohkoshi, *J. Mater. Chem. C*, 2018, **6**, 8372.

[S5] R. Herchel, Z. Travnicek and R. Zboril, *Inorg. Chem.*, 2011, **50**, 12390.

X-ray crystallography

The crystalline objects of **1**–**4** were selected for the single-crystal X-ray diffraction analyses from the mother solution, dispersed in Apiezon® N grease, mounted on Micro Mounts™ holder, and measured at room temperature, T = 293 K, using Bruker D8 Quest Eco Photon50 CMOS diffractometer equipped with graphite monochromated Mo Kα radiation. The data reduction and cell refinement were performed using SAINT and SADABS programs. The absorption correction was executed using a multi-scan procedure.

All crystal structures were solved by an intrinsic phasing method using a SHELXT, and refined following a weighted full-matrix least-square method on F^2 on SHELX-2014/7.[S6] Refinement was conducted using a WinGX (ver. 2014.1) integrated software. All non-hydrogen atoms were refined anisotropically. Hydrogen atoms of the 4,4'-bpdo ligands were calculated on the idealized positions, and refined using a riding model. Hydrogen atoms of water molecules and hydroxide U–OH–U bridges were found from the residual electron density map, and refined isotropically. In **1** and **3**, only single restraints on the O–H distances of U–OH–U bridges were applied. The crystal structures of **2** and **4** exhibit significantly higher structural disorder related mainly to crystallization water molecules, and terminal cyanide ligands. Therefore, a series of restraints were applied to maintain the proper geometry, and to ensure the convergence of the refinement procedure. In **2**, the DELU and ISOR restraints were applied on O atoms of water molecules and carbon atoms of selected cyanides, along with the DFIX command on the O–H distances of U–OH–U bridges. In **4**, the ISOR restraints were used for O atoms of water molecules, and some C atoms of cyanides, while the DFIX commands were necessary to stabilized the positions of hydrogen atoms of water molecules and hydroxide bridges. Details of crystal data and structure refinement were gathered in Table S1, when the detailed structure parameters are depicted in Table S2. CCDC reference numbers are 1857914, 1857915, 1857916, and 1857917, for **1**–**4**, respectively.

[S6] G. M. A. Sheldrick, *Acta Crystallogr., Sect. A: Found. Crystallogr.*, 2008, **64**, 112.

Physical techniques

A FTIR microscope, Nicolet iN10 MX was used to measure infrared absorption spectra on the selected single crystals. Raman spectra of the powder samples were collected using FT-Raman Bruker spectrometer (Model RFS 100) equipped with Nd:YAG laser (1064 nm, power of 40 mW) and Ge detector. CHN elemental analyses were performed on an Elementar Vario Micro Cube CHNS analyser. A PANalytical X'Pert PRO MPD diffractometer with a capillary spinning add-on, and Cu Kα radiation source was used to record the PXRD patterns on the air-dried polycrystalline samples. UV-Vis-NIR absorption spectra were collected in a transmission mode for the thin films of powder samples dispersed with a paraffin oil between two quartz plates, by using a PerkinElmer Lambda 35 spectrophotometer.

Photoluminescent properties were investigated at the temperature of liquid nitrogen using a FS5 spectrofluorometer (Edinburgh Instruments) equipped with an excitation source in form of an Xe (150 W) arc lamp, and R928P Hamamatsu photomultiplier as a signal detector. The powder samples were placed on the bottom of the NMR quartz tubes, and inserted in the optical cryostat. The background correction, taking into account the corrections from the lamp and the optical system characteristics, was performed within the Fluoracle® Software (Edinburgh Instruments).

Calculations

Continuous Shape Measure Analysis for the coordination sphere of seven-coordinated U^{VI} complexes in **1–4** was performed using a SHAPE software ver. 2.1.[S7]

[S7] (*a*) M. Llunell, D. Casanova, J. Cirera, J. Bofill, P. Alemany, S. Alvarez, M. Pinsky, D. Avnir, *SHAPE v. 2.1. Program for the Calculation of Continuous Shape Measures of Polygonal and Polyhedral Molecular Fragments*, University of Barcelona: Barcelona, Spain, 2013; (*b*) D. Casanova, J. Cirera, M. Llunell, P. Alemany, D. Avnir and S. Alvarez, *J. Am. Chem. Soc*., 2004, **126**, 1755.

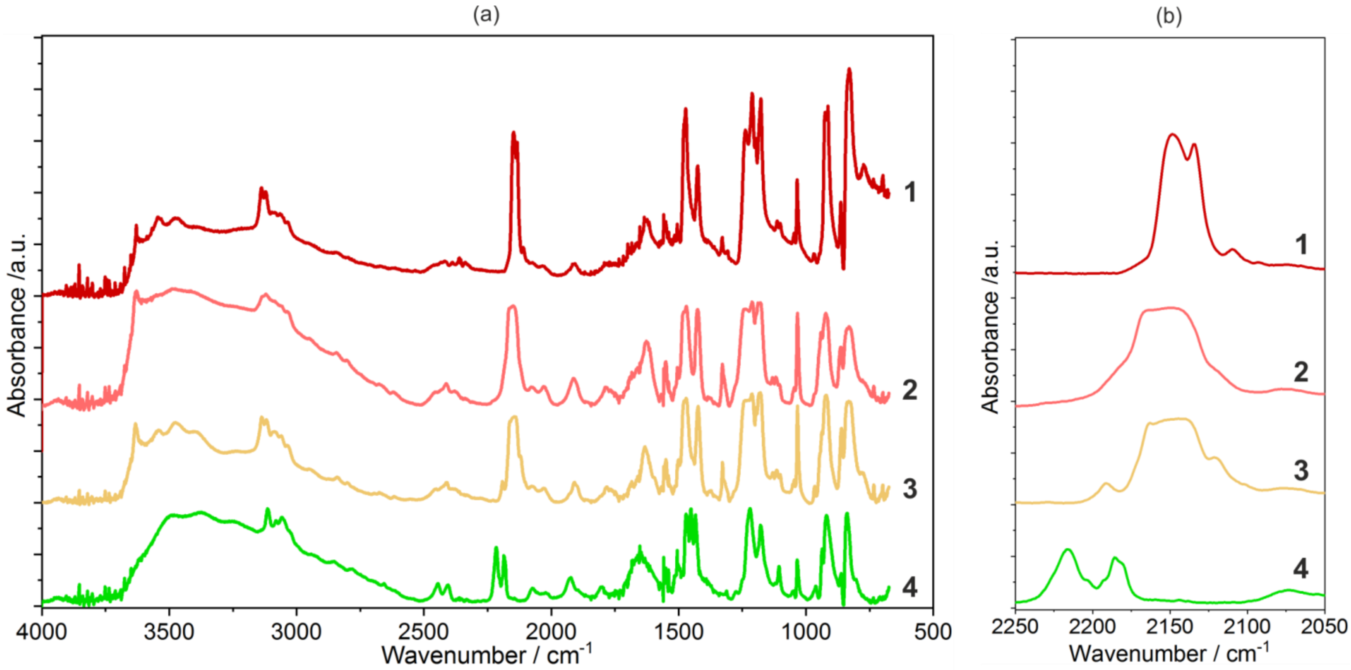

Figure S1. Infrared absorption spectra of the selected single crystals of **1**–**4** collected in the 4000–700 cm^{-1} range (*a*), and the enlargement of the 2250–2050 cm^{-1} region related to the stretching vibrations of cyanides (*b*).

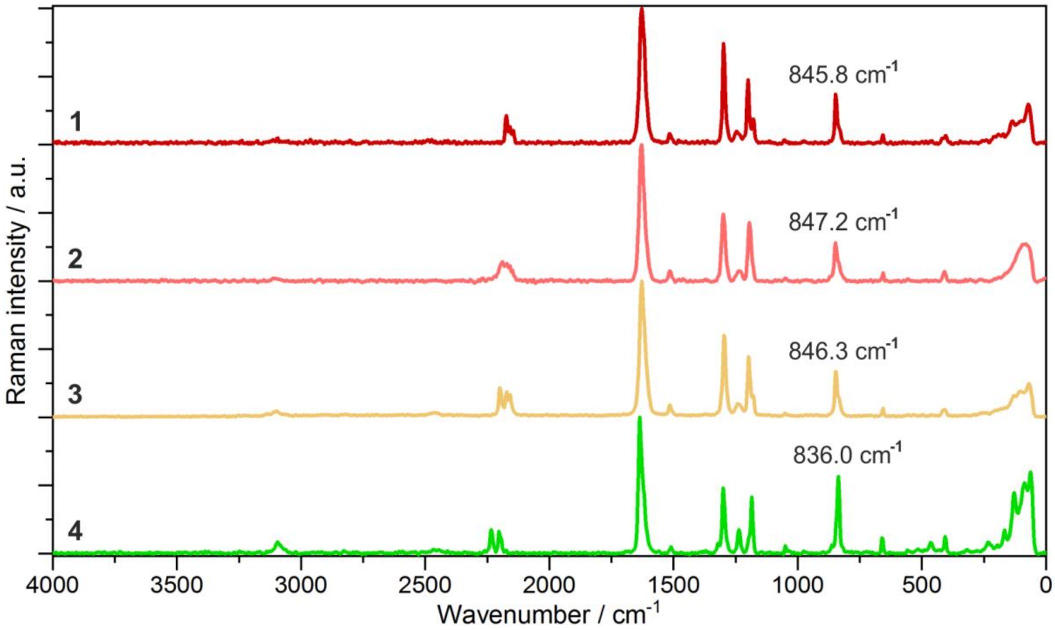

Figure S2. Raman spectra of the powder samples of **1**–**4** collected in the 4000–50 cm^{-1} range. The peaks with the indicated values from the 836–848 cm^{-1} range can be assigned to the symmetric stretching vibration of the $[OUO]^{2+}$ ions. These vibrational modes are responsible for the main splitting of the emission signal which is visible in the average energy differences of the $S_{10} \rightarrow S_{0v}$ emission components (Table S6).

Table S1. Crystal data and structure refinement for **1–4**.

Compound	**1**	**2**	**3**	**4**
formula	$U_4Co_2C_{52}H_{34}N_{20}O_{19}$	$U_4Rh_2C_{52}H_{34}N_{20}O_{18.2}$	$U_4Ir_2C_{52}H_{34}N_{20}O_{19}$	$U_2Pt_1C_{26}H_{20}N_{10}O_{11}$
formula weight [$g \cdot mol^{-1}$]	2312.97	2388.13	2579.51	1319.67
T [K]	293(2)			
λ [Å]	0.71073			
crystal system	orthorhombic			monoclinic
space group	P ccn (no. 56)			C 2/m (no. 12)
$\boldsymbol{a}$ [Å]	15.295(10)	15.1624(11)	15.3955(13)	12.005(2)
$\boldsymbol{b}$ [Å]	15.702(11)	15.9478(11)	15.9373(13)	15.276(3)
$\boldsymbol{c}$ [Å]	12.864(6)	12.7421(10)	12.8288(11)	9.8911(16)
$\boldsymbol{\alpha}$ [deg]	90	90	90	90
$\boldsymbol{\beta}$ [deg]	90	90	90	106.734(4)
$\boldsymbol{\gamma}$ [deg]	90	90	90	90
V [Å^3]	3090(3)	3081.1(4)	3147.7(5)	1737.0(5)
Z	2	2	2	2
calculated density [$g \cdot cm^{-3}$]	2.486	2.574	2.722	2.523
absorption coefficient [cm^{-1}]	11.059	11.086	14.552	13.387
F(000)	2120	2179.2	2320	1192
crystal size [mm × mm × mm]	0.15 × 0.05 × 0.04	0.08 × 0.03 × 0.03	0.13 × 0.06 × 0.04	0.17 × 0.17 × 0.08
crystal type	yellow needle	yellow needle	yellow needle	yellow plate
Θ range [deg]	2.442–24.947	2.448–25.027	2.646–25.681	3.426–27.475
limiting indices	$-18 < h < 18$ $-18 < k < 18$ $-15 < l < 15$	$-18 < h < 18$ $-18 < k < 18$ $-15 < l < 15$	$-18 < h < 18$ $-19 < k < 19$ $-15 < l < 15$	$-14 < h < 15$ $-19 < k < 18$ $-11 < l < 12$
collected reflections	22518	29940	23232	4182
unique reflections	2588	2719	2992	2015
R_{int}	0.0640	0.1643	0.0943	0.0397
completeness [%]	0.992	1.000	0.999	0.981
max. and min. transmission	0.288 and 0.666	0.471 and 0.732	0.253 and 0.594	0.209 and 0.414
data/restraints/ parameters	2688/1/226	2719/28/226	2992/1/226	2015/19/135
GOF on F^2	1.205	1.013	1.084	1.075
final R indices	$R_1 = 0.0401$ [$I > 2\sigma(I)$] $wR_2 = 0.0926$ (all data)	$R_1 = 0.0556$ [$I > 2\sigma(I)$] $wR_2 = 0.1405$ (all data)	$R_1 = 0.0455$ [$I > 2\sigma(I)$] $wR_2 = 0.1186$ (all data)	$R_1 = 0.0489$ [$I > 2\sigma(I)$] $wR_2 = 0.1245$ (all data)
largest diff peak/hole	1.298/-2.435 e·Å^{-3}	3.298/-1.99 e·Å^{-3}	3.097/-2.55 e·Å^{-3}	3.844/-1.27 e·Å^{-3}

Table S2. Detailed structure parameters of **1–4**.

Parameter	**1**	**2**	**3**	**4**
Details of hexacyanidometallate complexes				
M1–C1	1.891(10) Å	2.051(17) Å	2.030(14) Å	2.010(17) Å
M1–C2	1.905(10) Å	2.016(17) Å	2.036(14) Å	2.00(2) Å
M1–C3	1.910(12) Å	2.131(17) Å	2.035(17) Å	2.08(2) Å
M1–C1–N1	174.6(9)°	173.7(14)°	173.4(12)°	180°
M1–C2–N2	175.6(9)°	176.4(15)°	175.4(11)°	180.0(19)°
M1–C3–N3	176.3(10)°	175(3)°	178.1(13)°	179(2)°
C1–M1–C2	87.4(4)°	85.3(6)°	87.8(5)°	90.000(2)°
C1–M1–C3	87.7(5)°	87.2(7)°	87.1(6)°	90.000(3)°
C2–M1–C3	89.9(4)°	89.5(6)°	89.9(5)°	89.4(8)°
M1–U1 distance	5.440 Å 5.458 Å	5.440 Å 5.526 Å	5.464 Å 5.535 Å	5.710 Å
Details of uranyl complexes				
U1–O1	1.794(8) Å	1.788(11) Å	1.778(10) Å	1.760(9) Å
U1–O2	1.777(8) Å	1.704(12) Å	1.761(9) Å	2.376(9) Å
U1–O3	2.339(5) Å	2.295(7) Å	2.316(6) Å	2.345(8) Å
U1–O4	2.340(7) Å	2.353(10) Å	2.357(9) Å	-
U1–O5	2.396(7) Å	2.394(9) Å	2.392(8) Å	-
U1–N1	2.536(9) Å	2.503(13) Å	2.495(10) Å	2.622(14) Å
U1–N2	2.538(9) Å	2.513(15) Å	2.482(11) Å	-
U1–O3–U1	128.8(5)°	129.1(7)°	128.8(6)°	110.6(6)°
U1–N1–C1	159.7(8)°	159.2(13)°	160.1(11)°	180°
U1–N2–C2	158.5(8)°	156.8(14)°	154.7(11)°	-
U1–O4–N4	127.0(6)°	128.3(9)°	128.2(8)°	130.7(7)° (O2-N4)
U1–O5–N5	139.8(6)°	138.9(8)°	139.3(7)°	-
N1–U1–N2	145.8(3)°	146.5(4)°	144.9(4)°	-
N1–U1–O1	88.1(3)°	89.1(5)°	87.6(4)°	87.7(3)°
N1–U1–O2	92.0(3)°	91.5(5)°	94.0(4)°	70.4(2)°
N1–U1–O3	72.9(2)°	72.5(3)°	72.6(3)°	145.3(3)°
N1–U1–O4	73.2(3)°	73.4(4)°	72.8(3)°	-
N1–U1–O5	144.0(3)°	144.5(4)°	144.5(3)°	-
N2–U1–O1	90.7(3)°	89.9(5)°	88.9(4)°	-
N2–U1–O2	88.0(3)°	89.1(5)°	88.6(5)°	-
N2–U1–O3	141.4(2)°	141.0(3)°	142.4(3)°	-
N2–U1–O4	72.6(3)°	73.2(4)°	72.3(4)°	-
N2–U1–O5	70.0(3)°	68.7(4)°	70.1(4)°	-
O1–U1–O2	177.9(4)°	179.0(6)°	177.4(5)°	87.5(4)°; 91.0(4)°
O1–U1–O3	91.1(3)°	90.8(5)°	90.1(4)°	90.9(5)°; 92.8(5)°
O1–U1–O4	89.7(3)°	91.3(5)°	90.9(4)°	175.4(6)° (O1-O1)
O1–U1–O5	87.0(3)°	86.4(4)°	87.2(4)°	-
O2–U1–O3	91.0(3)°	90.2(5)°	92.3(5)°	75.0(4)°; 144.3(4)°
O2–U1–O4	88.2(3)°	88.1(5)°	87.6(4)°	140.7(5)° (O2-O2)
O2–U1–O5	94.2(3)°	93.5(5)°	92.7(4)°	-
O3–U1–O4	146.0(2)°	145.8(3)°	145.3(2)°	69.4(6)° (O3-O3)
O3–U1–O5	71.59(19)°	72.4(3)°	72.3(2)°	-
O4–U1–O5	142.3(3)°	141.8(4)°	142.4(3)°	-

Table S3. Bond valence sums (BVS) of uranium and oxygen centres in **1–4**.*

Atom	**1**	**2**	**3**	**4**
U1	6.68	7.29	6.97	6.77
O1	2.14	2.17	2.23	2.35
O2	2.24	2.72	2.33	-
O3	0.98	1.10	1.04	0.97

* BVS sums showing the atom valency, V_i were calculated using the following equation:

$$V_i = \sum_j \exp\left(\frac{r_0 - r_{ij}}{b}\right)$$

where r_0 is the bond-valence parameter for a given pair of atoms, determined from the average bond lengths of a large number of experimental crystal structures. Recommended bond-valence parameters for U–O and U–N are 2.075 Å and 2.24 Å, respectively. The r_{ij} parameters are the experimental bond lengths between atoms *i* and *j*, and the *b* parameter is a 'universal' constant equal to 0.37 Å.[S8]

Comment to Table S3:

Determined bond valence sums indicate the high oxidation state of uranium cations in all compounds, **1–4**. It can be assigned to +VI, even that the related atom valencies are within the higher range of 6.6–7.3.[S9] The bond valence sums for O1 and O2 atoms are higher than 2 proving the oxido, O^{2-} character of these anions. The bridging O3 atoms are characterized by much lower atom valencies close to 1, suggesting that they are of a hydroxyl, OH^- character, which is in a good agreement with the charge balance in compounds **1–4**. However, it does not exclude the possible equimolar mixture of oxide and aqua ligands which may exist at this crystallographic position, or even the mixture of all form (oxide, hydroxide and aqua) which together can give the average bond valency close the unity. Bond valence summations cannot undoubtedly expel such interpretation, especially when it is suggested by the broadening of the uranyl-based emission band (see the discussion on the emission properties).[S8b, S10]

[S8] (*a*) N. E. Breese and M. O'Keeffe, *Acta Cryst.*, 1991, **B47**, 192; (*b*) Y. Zhang, J. K. Clegg, K. Lu, G. R. Lumpkin, T. T. Tran, I. Aharonovich, N. Scales and F. Li, *ChemistrySelect*, 2016, **1**, 7.

[S9] P. C. Burns, R. C. Ewing and F. C. Hawthorne, *Can. Mineral.*, 1997, **35**, 1551.

[S10] Y. Zhang, M. Bhadbhade, I. Karatchevtseva, J. R. Price, H. Liu, Z. Zhang, L. Kong, J. Cejka, K. Lu and G. R. Lumpkin, *J. Solid State Chem.*, 2015, **226**, 42.

Table S4. Results of Continuous Shape Measure Analysis for uranyl complexes[#] in the crystal structures of **1**–**4**.

Compound	CSM parameters*			Geometry
	PBPY-7	COC-7	CTPR-7	
1	1.850	8.928	7.141	PBPY-7
2	1.977	9.274	7.443	PBPY-7
3	1.788	9.326	7.575	PBPY-7
4	1.904	9.478	7.631	PBPY-7

[#] Uranyl complexes in **1**–**3** are of the composition of $[UO_2(\mu\text{-}4,4'\text{-bpdo})_2(\mu\text{-OH})(\mu\text{-NC})_2]^-$, while uranyl complex in **4** exhibits the composition of $[UO_2(\mu\text{-}4,4'\text{-bpdo})_2(\mu\text{-OH})_2(\mu\text{-NC})]$.

* CSM parameters:[S7]
CSM PBPY-7 = the parameter related to the pentagonal bipyramid geometry (D_{5h} symmetry)
CSM COC-7 = the parameter related to the capped octahedron geometry (C_{3v} symmetry)
CSM CTPR-7 = the parameter related to the capped trigonal prism geometry (C_{2v} symmetry)
CSM = 0 for the ideal geometry and the increase of CSM parameter corresponds to the increasing distortion from the ideal polyhedron.

Table S5. Detailed interatomic distances of hydrogen bonding network of **1**–**4**.

Hydrogen bonds	**1**	**2**	**3**
O1S-N3	3.16 Å	3.24 Å	3.10 Å
O1S-O4	3.53 Å	3.61 Å	3.61 Å
O3-(H3)-O2	4.18 Å	4.18 Å	4.15 Å

Hydrogen bonds	**4**
O1S-(H1A)-N2	2.85 Å
O1S-(H1B)-O3	2.84 Å
O3-(H3A)-N3	3.23 Å

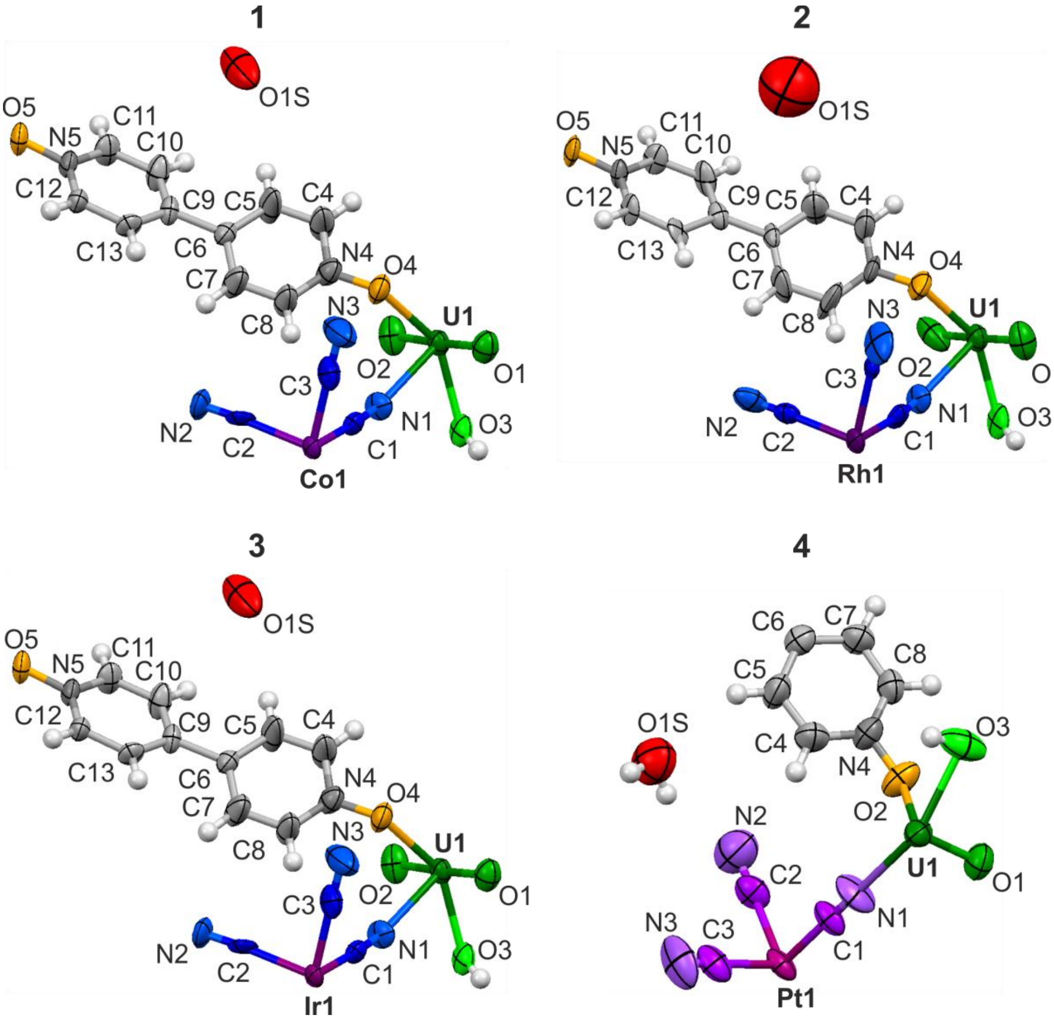

Figure S3. Comparison of the asymmetric units of **1**–**4** with the atoms labelling schemes. Thermal ellipsoids are shown at the 70% probability level. The related bond lengths and angles are gathered in Table S2.

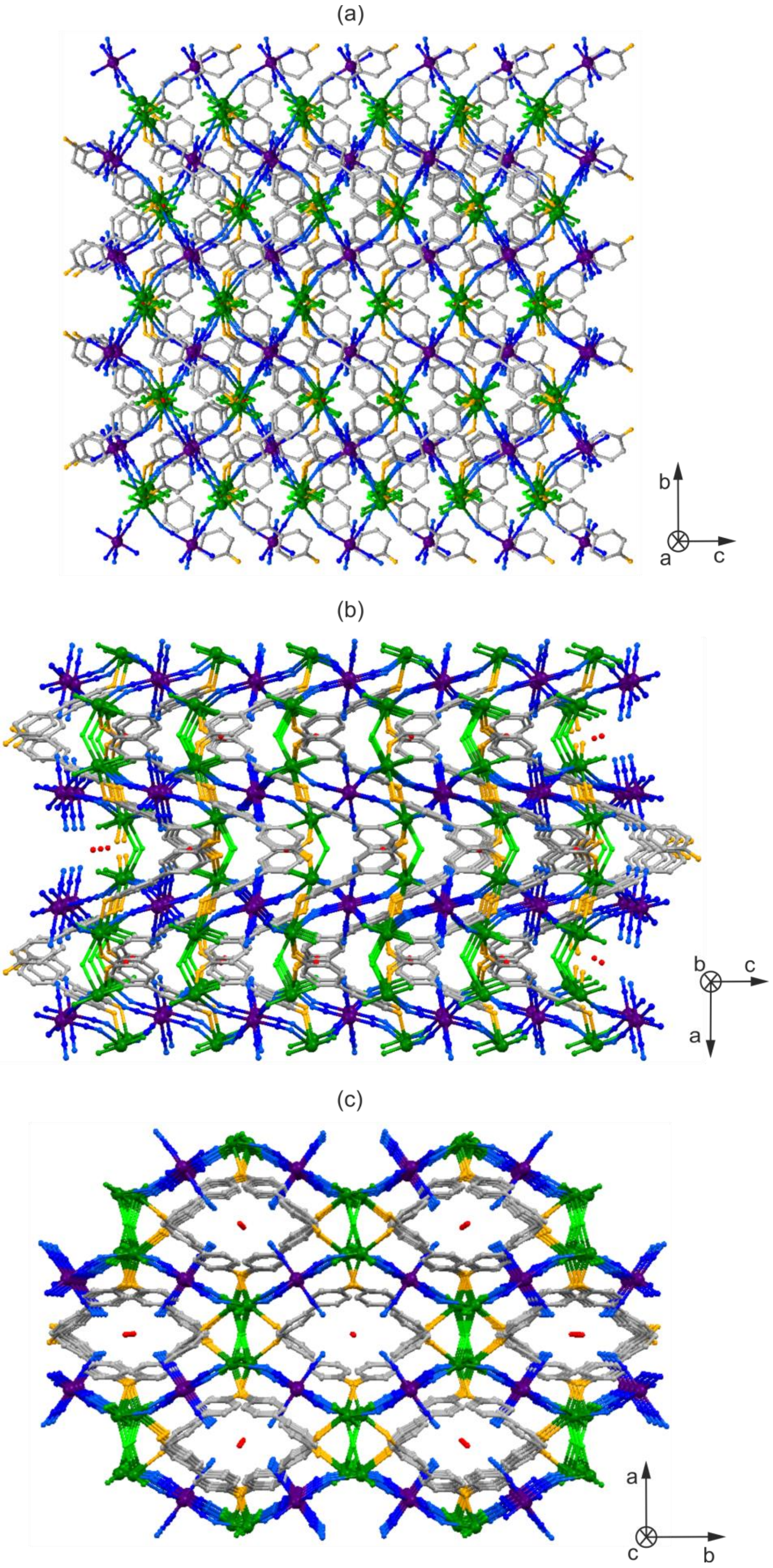

Figure S4. The views of the three-dimensional coordination network and crystallization water molecules in the crystal structure of **1** along three main crystallographic axes: (a) the *a* axis, (b) the *b* axis, and (c) the *c* axis. The supramolecular networks of **2** and **3** are essentially identical due to their isostructurality with **1**.

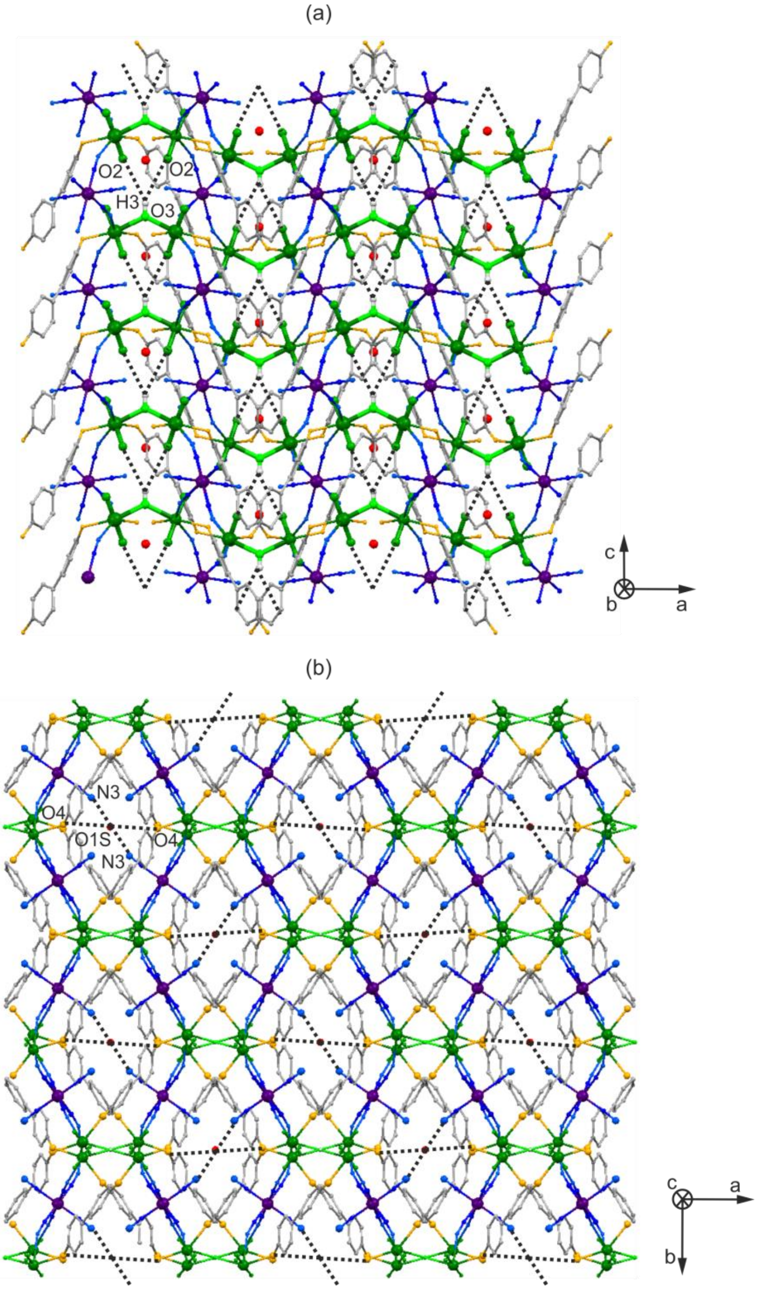

Figure S5. Hydrogen bonding network in **1** showing two sets of hydrogen bonds involving hydroxide molecular bridges and uranyl cations within the *ac* plane (a), and related to the crystallization water molecules interacting with terminal cyanides and O-atoms of 4,4'-bpdo ligands within the *ab* plane (b). The dotted lines represent the hydrogen bonds. The interatomic distances related to the presented non-covalent interactions are gathered in Table S4.

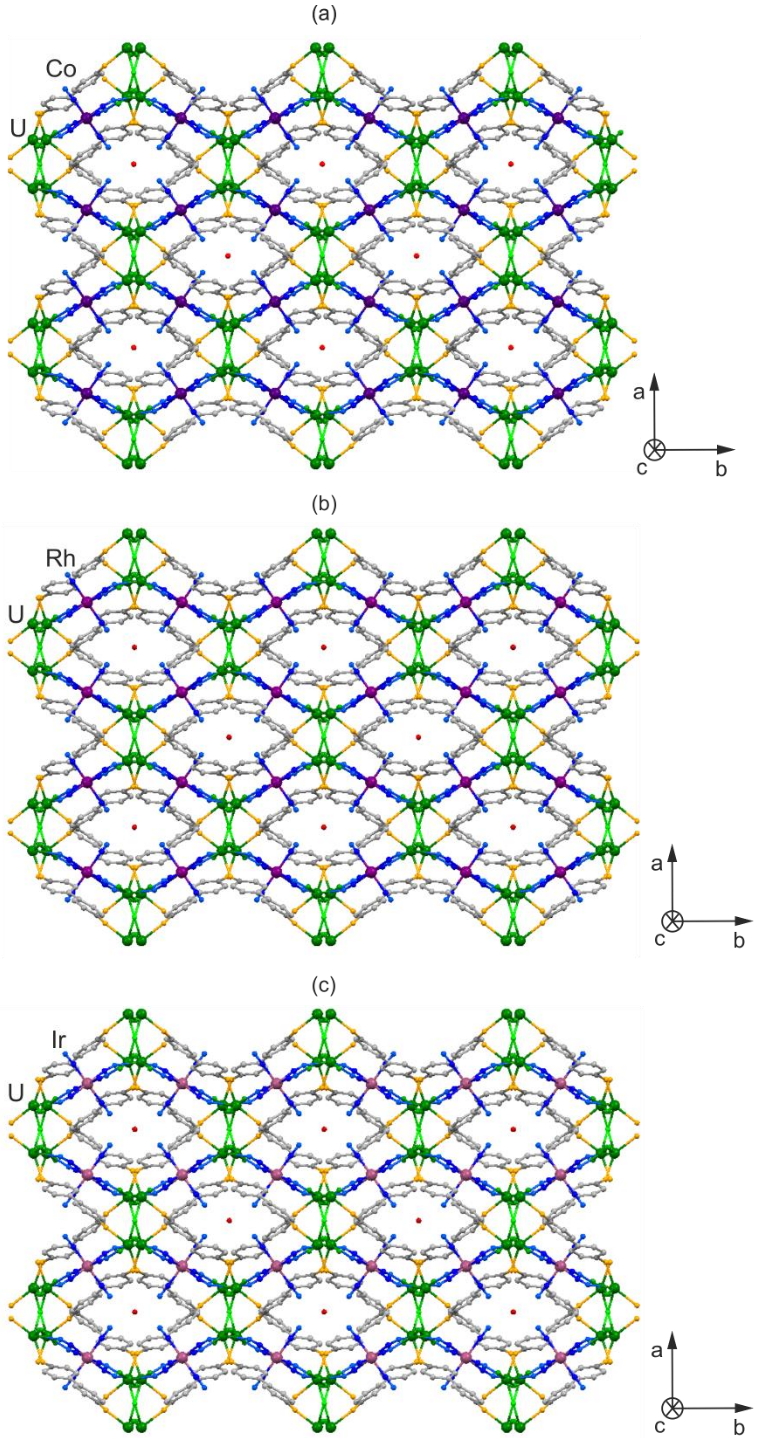

Figure S6. Comparison of the representative views of the three-dimensional coordination frameworks of **1** (a), **2** (b), and **3** (c) presented within the *ab* crystallographic plane.

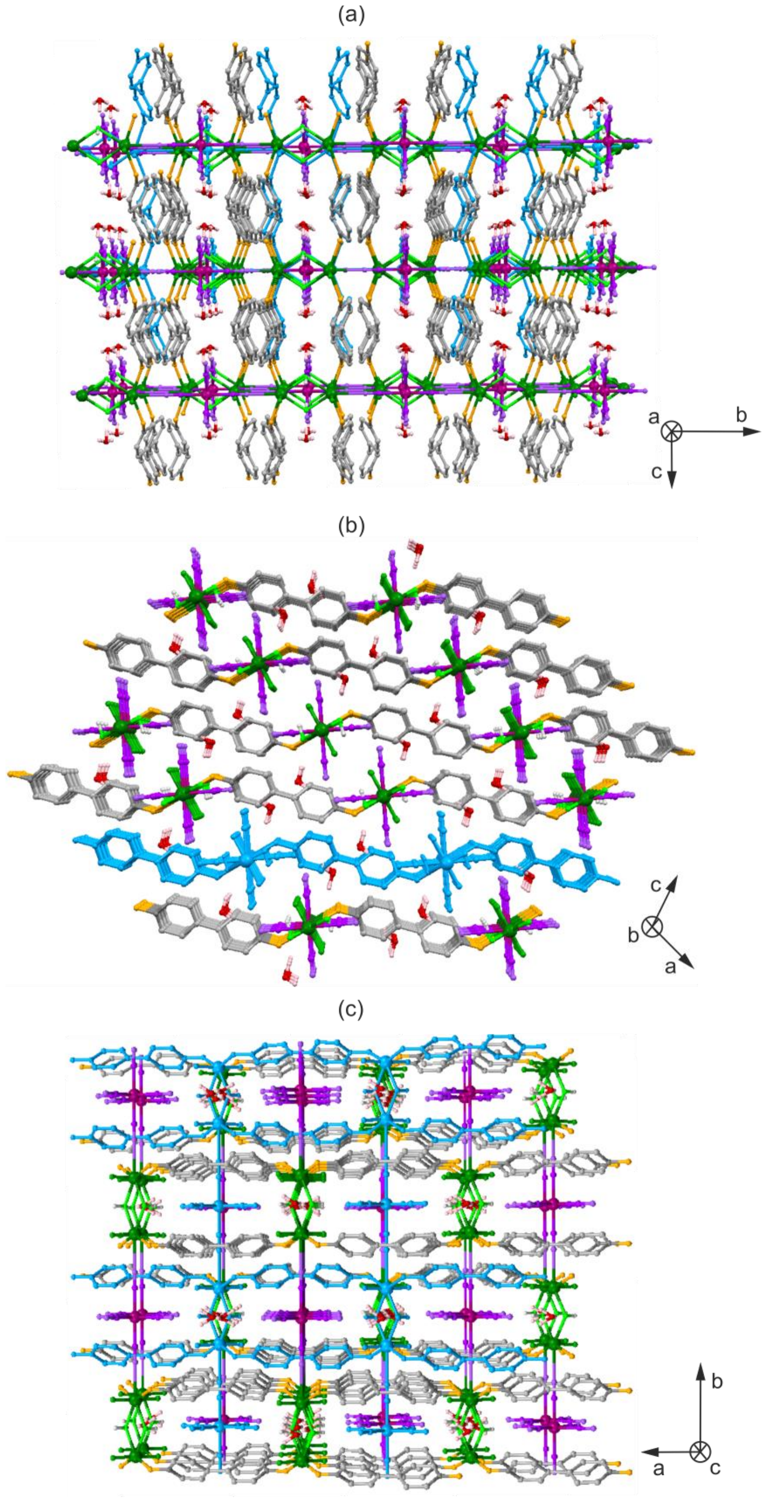

Figure S7. The views of the supramolecular network of **4** along three main crystallographic axes: (a) the *a* axis, (b) the *b* axis, and (c) the *c* axis. A representative coordination layer was shown using blue colour.

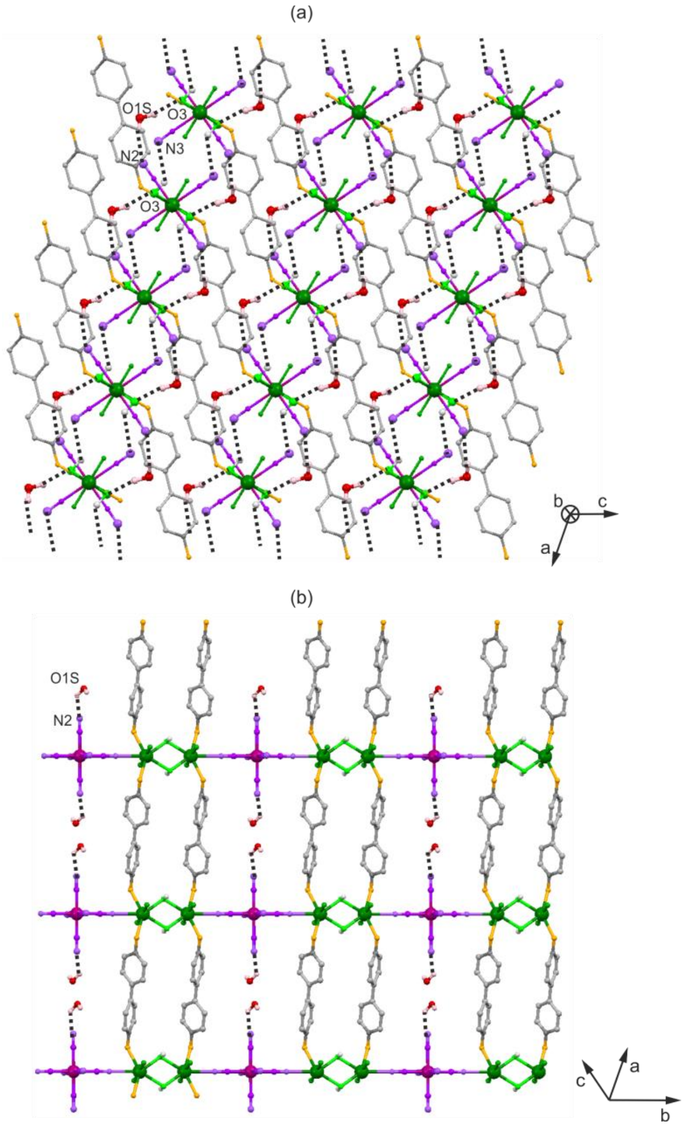

Figure S8. Hydrogen bonding network in **4** involving crystallization water molecules (O1S), terminal cyanides (N2, N3) and hydroxide bridges (O3), presented within the *ac* plane (a), and the (101) plane (b). The dotted lines represent the hydrogen bonds. The interatomic distances related to the presented hydrogen bonds are collected in Table S4.

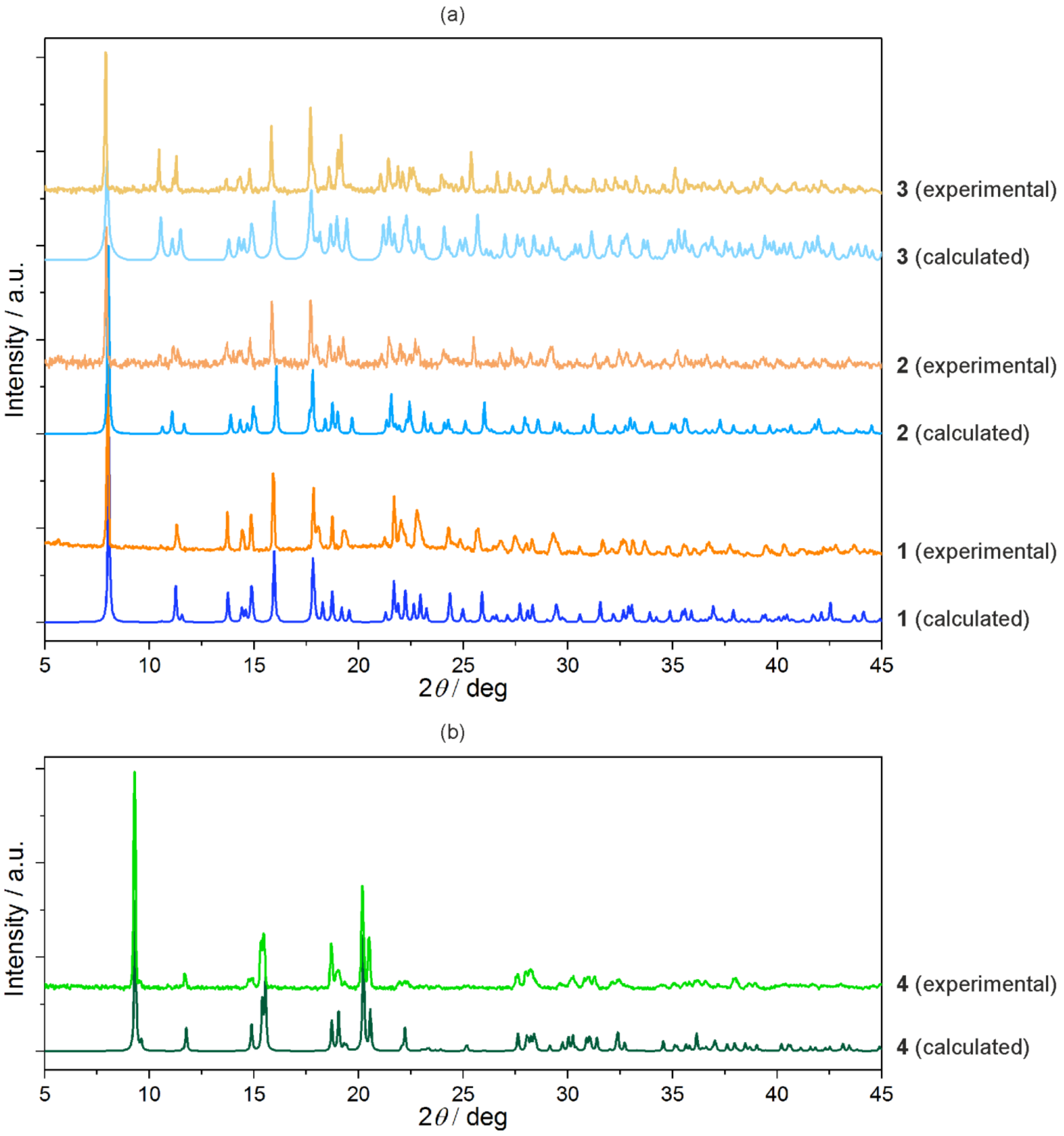

Figure S9. Experimental powder X-ray diffraction (PXRD) patterns of the polycrystalline samples of isostructural compounds **1**–**3** (a), and compound **4** (b). The respective PXRD patterns calculated on the basis of the structural models achieved from the single-crystal X-ray (SC-XRD) structural analysis were also presented for comparison, indicating the phase purity of the obtained materials. Only the representative range of 5–45° of 2*Θ* angle is shown for clarity.

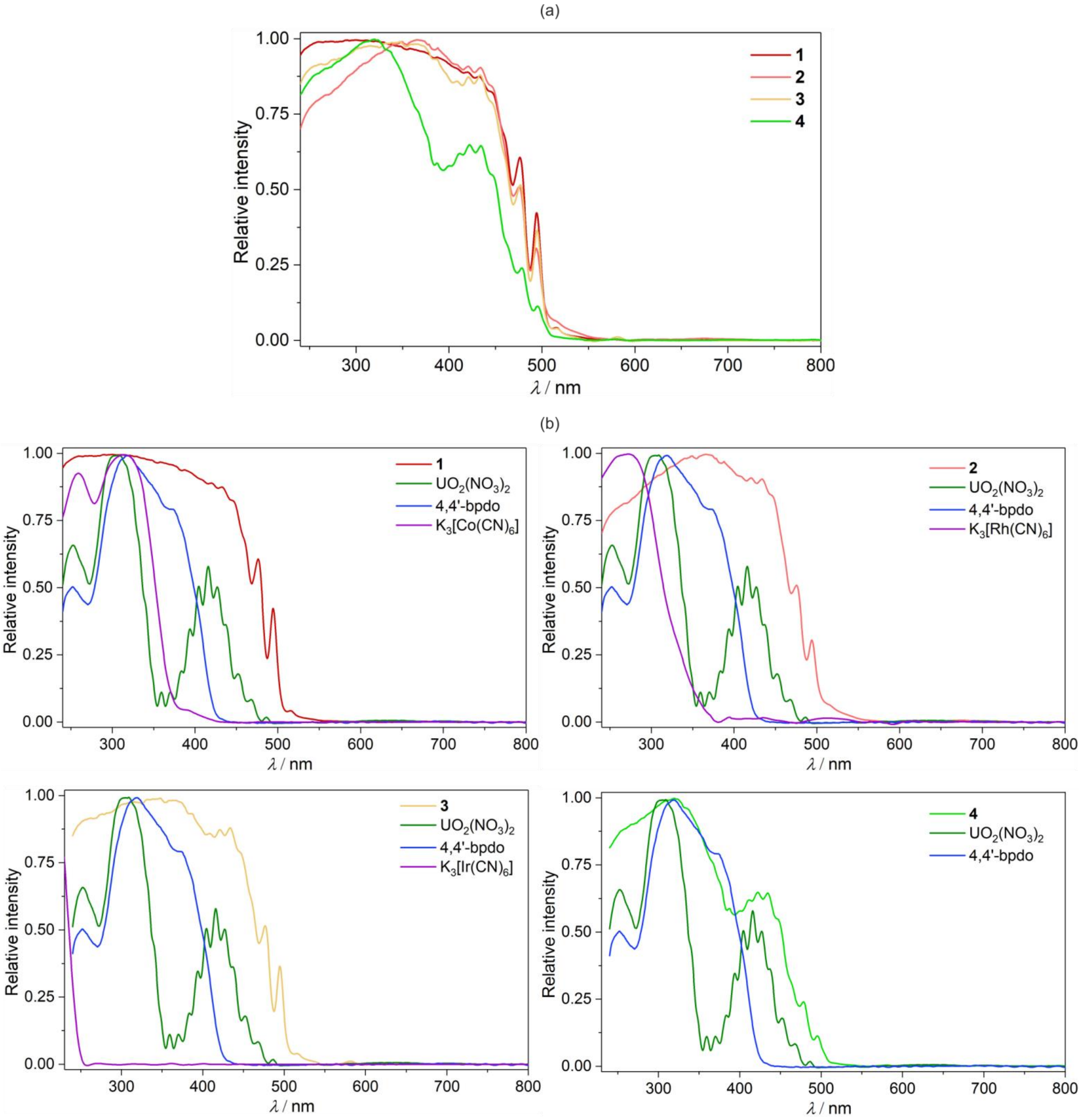

Figure S10. Solid state room temperature UV–Vis–NIR absorption spectra of **1**–**4**, presented all together (a), and separately along with the reference spectra of uranyl nitrate, 4,4'-bpdo, and the respective hexacyanidometllate precursors (b). In the case of compound **4** and its references, there is no spectrum of $K_2[Pt(CN)_6]$ as this metal cyanide precursor does not show any significant absorption above 240 nm, within the measurement range.[S11]

[S11] D. L. Swihart and W. Roy Mason, *Inorg. Chem.*, 1970, **9**, 1749.

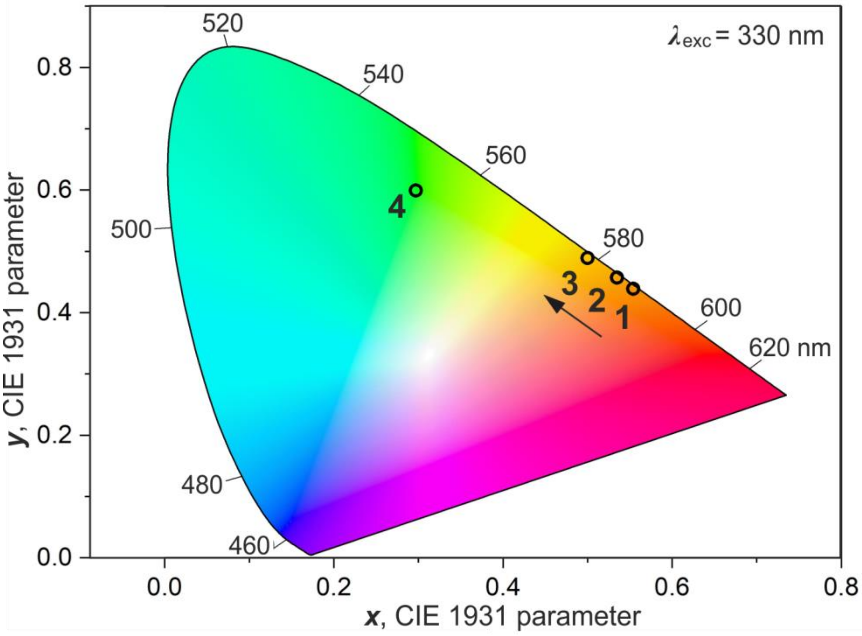

Figure S11. Emission colours of **1**–**4** shown on the CIE 1931 chromaticity diagram. The related *xy* parameters are: *x* = 0.558, *y* = 0.431 (**1**), *x* = 0.527, *y* = 0460 (**2**), *x* = 0.485, *y* = 0.501 (**3**), and *x* = 0.295, *y* = 0.602 (**4**).

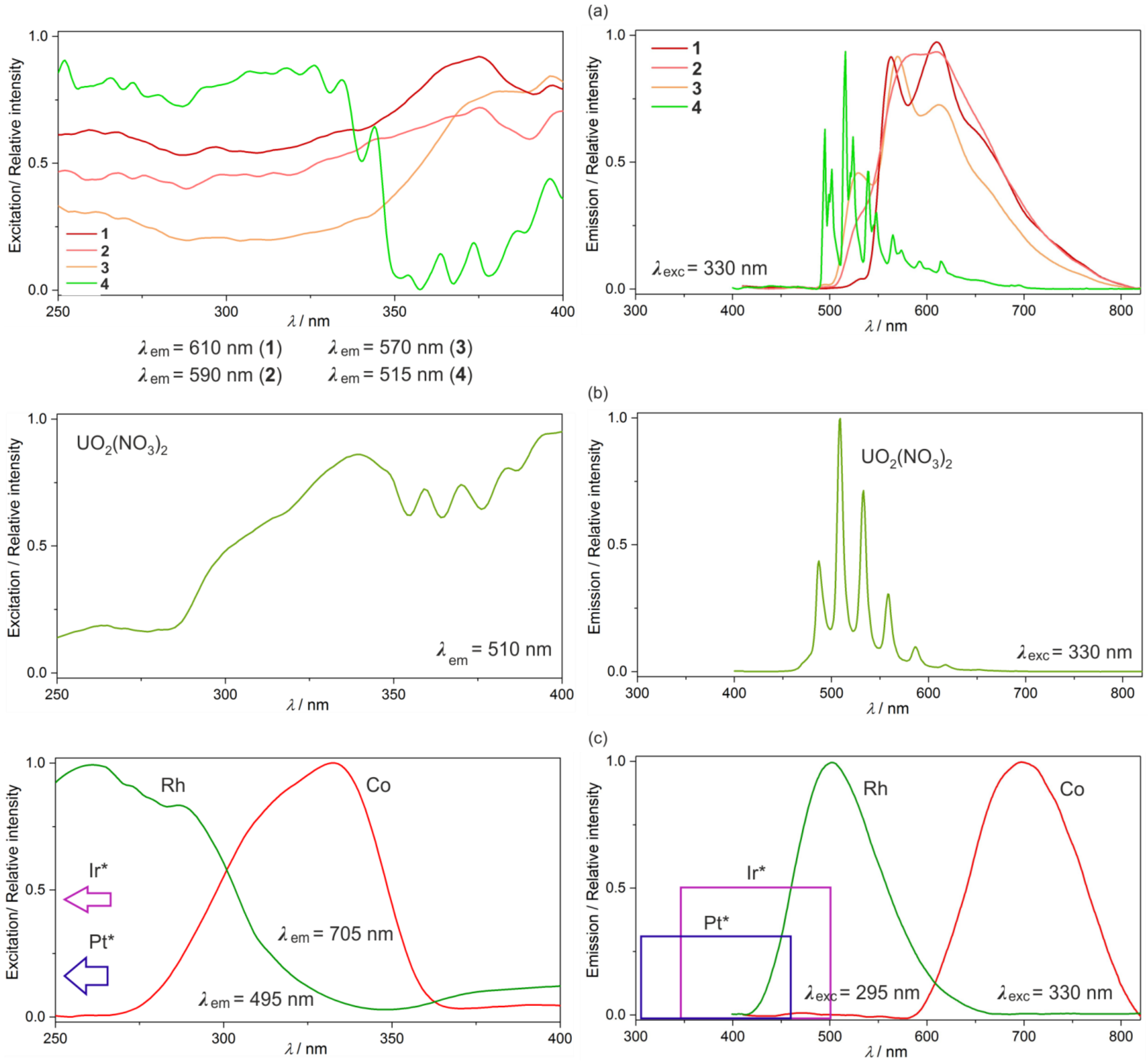

Figure S12. Solid state excitation (left panel) and emission (right panel) spectra of **1**–**4** (*a*) compared with the reference spectra of $UO_2(NO_3)_2$ (*b*), and $K_3[M^{III}(CN)_6]$ (M = Co, Rh, Ir) and $K_2[Pt^{IV}(CN)_6]$ salts (*c*), at the indicated excitation and emission wavelengths. All spectra were collected at liquid nitrogen temperature. In (*c*), the positions of emission and excitation bands of $K_3[Ir^{III}(CN)_6]$ and $K_2[Pt^{IV}(CN)_6]$ were postulated according to the literature reports.[S11–S12] These spectra could not be gathered in our measurement system due to the excitation moved below 250 nm.

[S12] A. Wölpl and D. Oelkrug, *Ber. Buns. Gessell.*, 1975, **79**, 394.

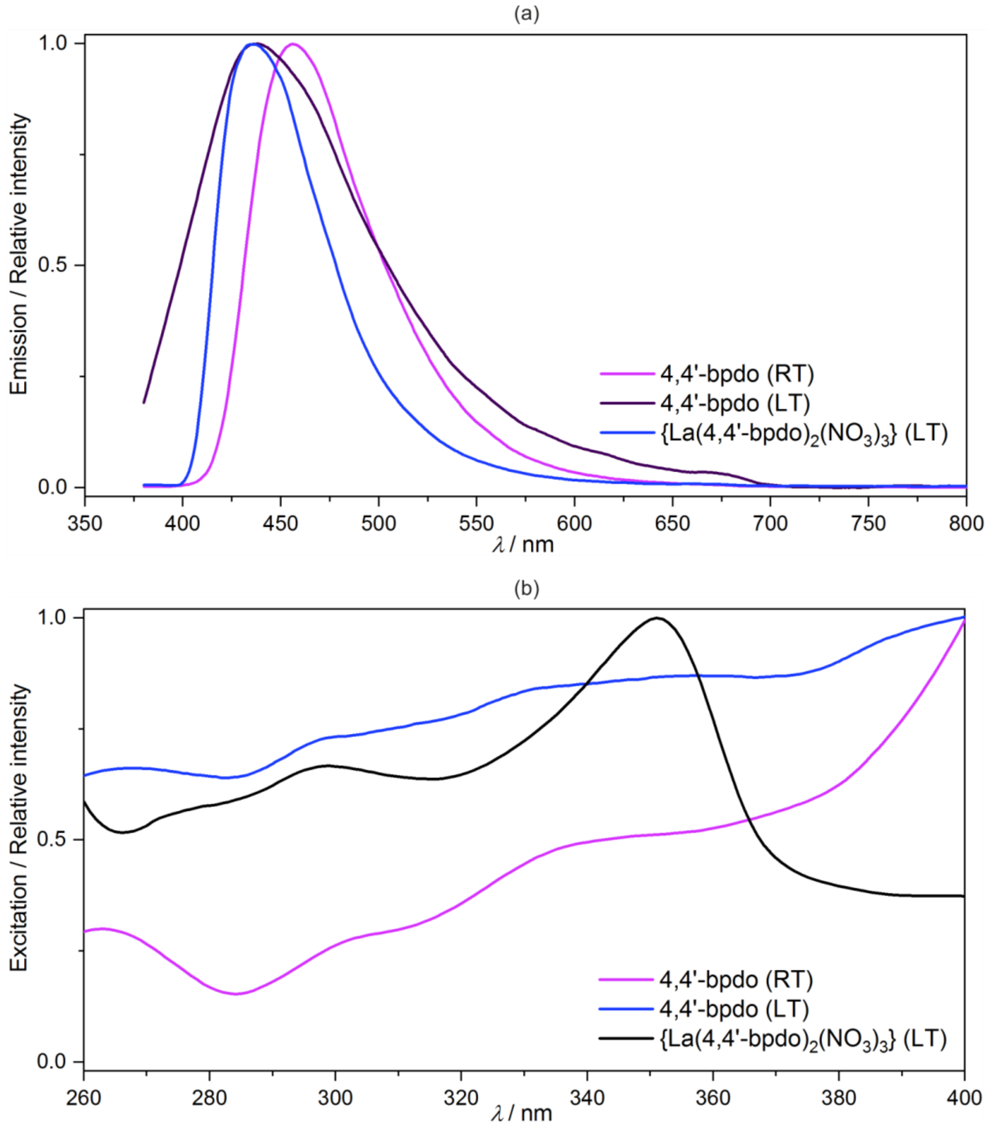

Figure S13. Solid state emission (*a*) and excitation (*b*) spectra of free 4,4'-bpdo ligand collected both at room (RT) and liquid nitrogen (LT) temperatures, and the related spectra of the {La(4,4'-bpdo)$_2$(NO$_3$)$_3$} coordination polymer, collected at liquid nitrogen (LT) temperature.[S13] The excitation wavelength of 330 nm was used for all emission spectra. The excitation spectra were gathered for the emission wavelengths of 456, 438 and 437 nm for 4,4'-bpdo (RT), 4,4'-bpdo (LT), and {La(4,4'-bpdo)$_2$(NO$_3$)$_3$} (LT), respectively.

[S13] R. J. Hill, D.-L. Long, M. S. Turvey, A. J. Blake, N. R. Champness, P. Hubberstey, C. Wilson and M. Schröder, *Chem. Commun*. 2004, 1792.

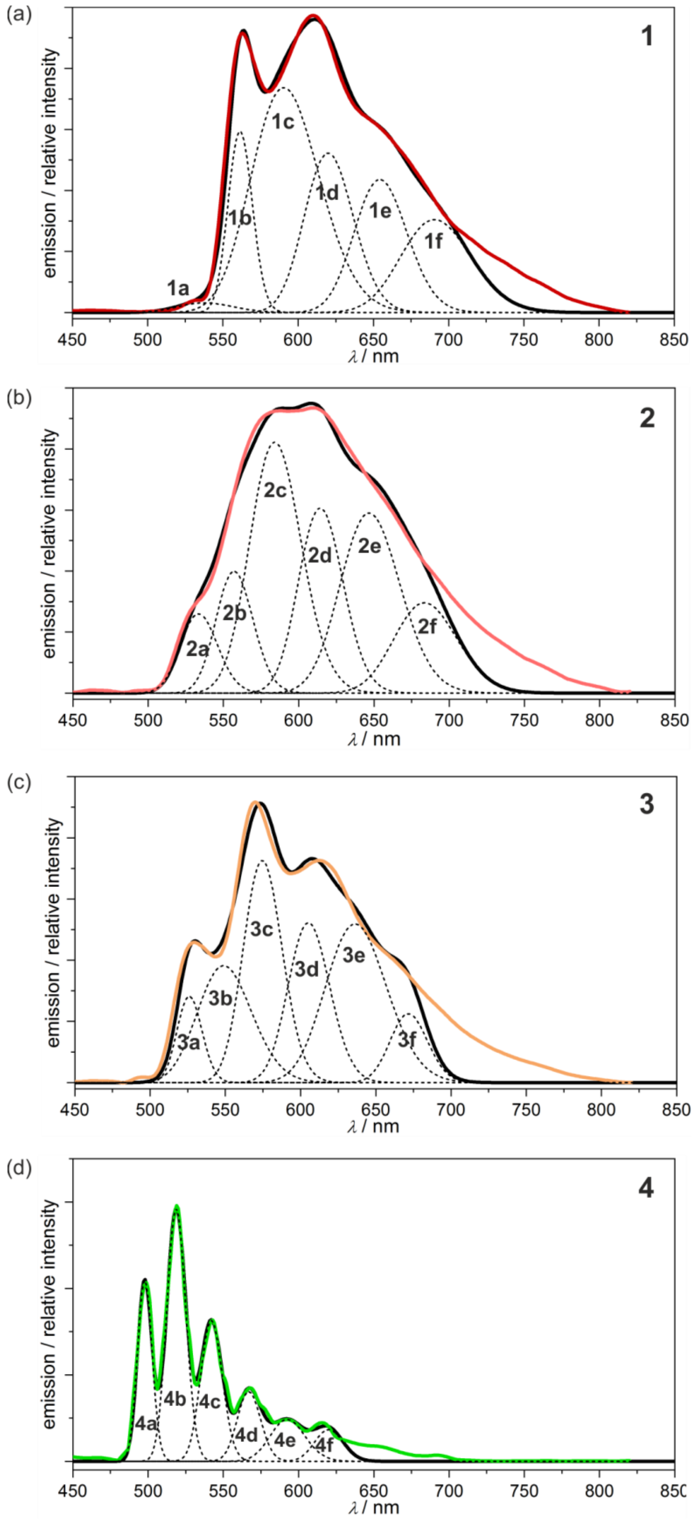

Figure S14. Deconvolution of the solid state emission spectra of **1** (a), **2** (b), **3** (c), and **4** (d) into six emission components (*a*–*f*) related to the electronic transitions within implemented uranyl complexes (Table S6). The spectra were gathered at liquid nitrogen temperature under the excitation of 330 nm light. The coloured lines represent the experimental data, the dotted black lines show the emission components, while the solid black lines indicate the calculated sums related to the best fits. The long wavelength emission tail was found in all the spectra, and left without the detailed analysis due to the presumable numerous emission peaks in this range. The low resolution spectrum was used for **4**, when all the other emission spectra are of the best possible resolution.

Table S6. Analysis of the solid state emission spectra of **1**–**4** (see Figure S14) including the list of identified emission peaks, the emission energies, and the energy differences between the peak positions.

Electronic transition of UO_2^{2+} ions[S14]	Compound							
	1		**2**		**3**		**4**	
	peak position	energy difference	peak position	energy difference	peak position	energy difference	peak position	energy difference
$S_{11} \rightarrow S_{00}$	peak **1a** 18595 cm^{-1} 537.8 nm	-	peak **2a** 18744 cm^{-1} 533.5 nm	-	peak **3a** 19010 cm^{-1} 526.0 nm	-	not observed	-
$S_{10} \rightarrow S_{00}$	peak **1b** 17813 cm^{-1} 561.4 nm	peaks **1a–1b** 782 cm^{-1}	peak **2b** 17952 cm^{-1} 557.0 nm	peaks **2a–2b** 792 cm^{-1}	peak **3b** 18219 cm^{-1} 549.9 nm	peaks **3a–3b** 791 cm^{-1}	peak **4a** 20132 cm^{-1} 496.8 nm	-
$S_{10} \rightarrow S_{01}$	peak **1c** 16936 cm^{-1} 590.5 nm	peaks **1b–1c** 877 cm^{-1}	peak **2c** 17122 cm^{-1} 584.0 nm	peaks **2b–2c** 830 cm^{-1}	peak **3c** 17400 cm^{-1} 574.7 nm	peaks **3b–3c** 819 cm^{-1}	peak **4b** 19280 cm^{-1} 518.7 nm	peaks **4a–4b** 852 cm^{-1}
$S_{10} \rightarrow S_{02}$	peak **1d** 16132 cm^{-1} 619.9 nm	peaks **1c–1d** 804 cm^{-1}	peak **2d** 16280 cm^{-1} 614.3 nm	peaks **2c–2d** 842 cm^{-1}	peak **3d** 16524 cm^{-1} 605.2 nm	peaks **3c–3d** 876 cm^{-1}	peak **4c** 18450 cm^{-1} 542.0 nm	peaks **4b–4c** 830 cm^{-1}
$S_{10} \rightarrow S_{03}$	peak **1e** 15285 cm^{-1} 654.2 nm	peaks **1d–1e** 847 cm^{-1}	peak **2e** 15462 cm^{-1} 646.7 nm	peaks **2d–2e** 818 cm^{-1}	peak **3e** 15720 cm^{-1} 636.1 nm	peaks **3d–3e** 804 cm^{-1}	peak **4d** 17640 cm^{-1} 566.9 nm	peaks **4c–4d** 810 cm^{-1}
$S_{10} \rightarrow S_{04}$	peak **1f** 14480 cm^{-1} 690.6 nm	peaks **1e–1f** 805 cm^{-1}	peak **2f** 14630cm^{-1} 683.5 nm	peaks **2e–2f** 832 cm^{-1}	peak **3f** 14889 cm^{-1} 671.6 nm	peaks **3e–3f** 831 cm^{-1}	peak **4e** 16880 cm^{-1} 592.4 nm	peaks **4d–4e** 760 cm^{-1}
$S_{10} \rightarrow S_{05}$	-	-	-	-	-	-	peak **4f** 16130 cm^{-1} 620.0 nm	peaks **4e–4f** 750 cm^{-1}
energy difference $S_{11} \rightarrow S_{00}$	-	**782 cm^{-1}**	-	**792 cm^{-1}**	-	**791 cm^{-1}**	-	-
average energy difference $S_{10} \rightarrow S_{0v}$	-	**834 cm^{-1}**	-	**831 cm^{-1}**	-	**831 cm^{-1}**	-	**801 cm^{-1}**

[S14] (*a*) P. Thuery, E. Riviere and J. Harrowfield, *Inorg. Chem.*, 2015, **54**, 2838; (*b*) R. Zhao, L. Mei, K.-Q. Hu, M. Tian, Z.-F. Chai and W.-Q. Shi, *Inorg. Chem.*, 2018, **57**, 6084.

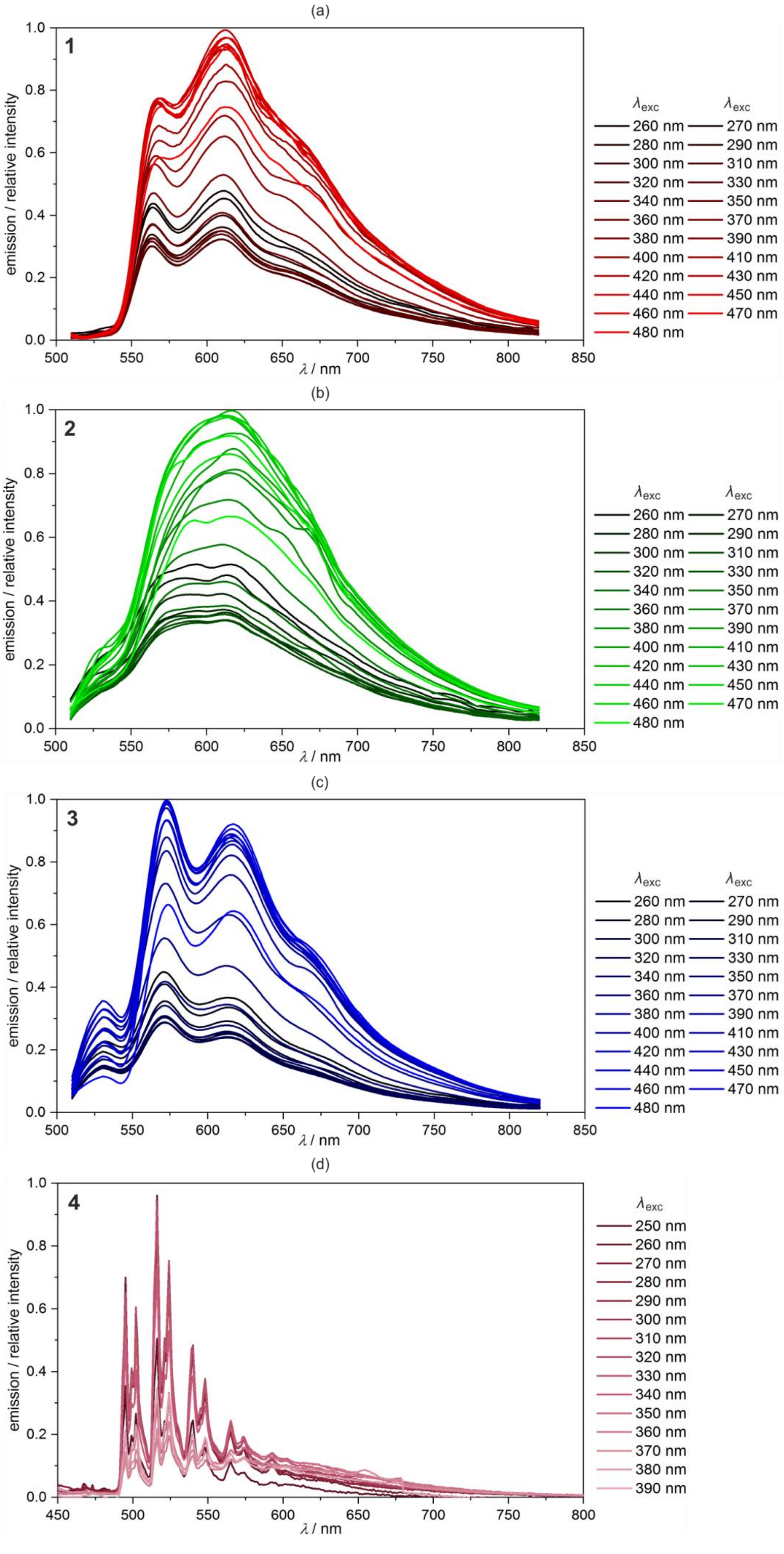

Figure S15. Solid state emission spectra of **1** (*a*), **2** (*b*), **3** (*c*), and **4** (*d*) collected at liquid nitrogen temperature under various indicated excitation wavelengths.

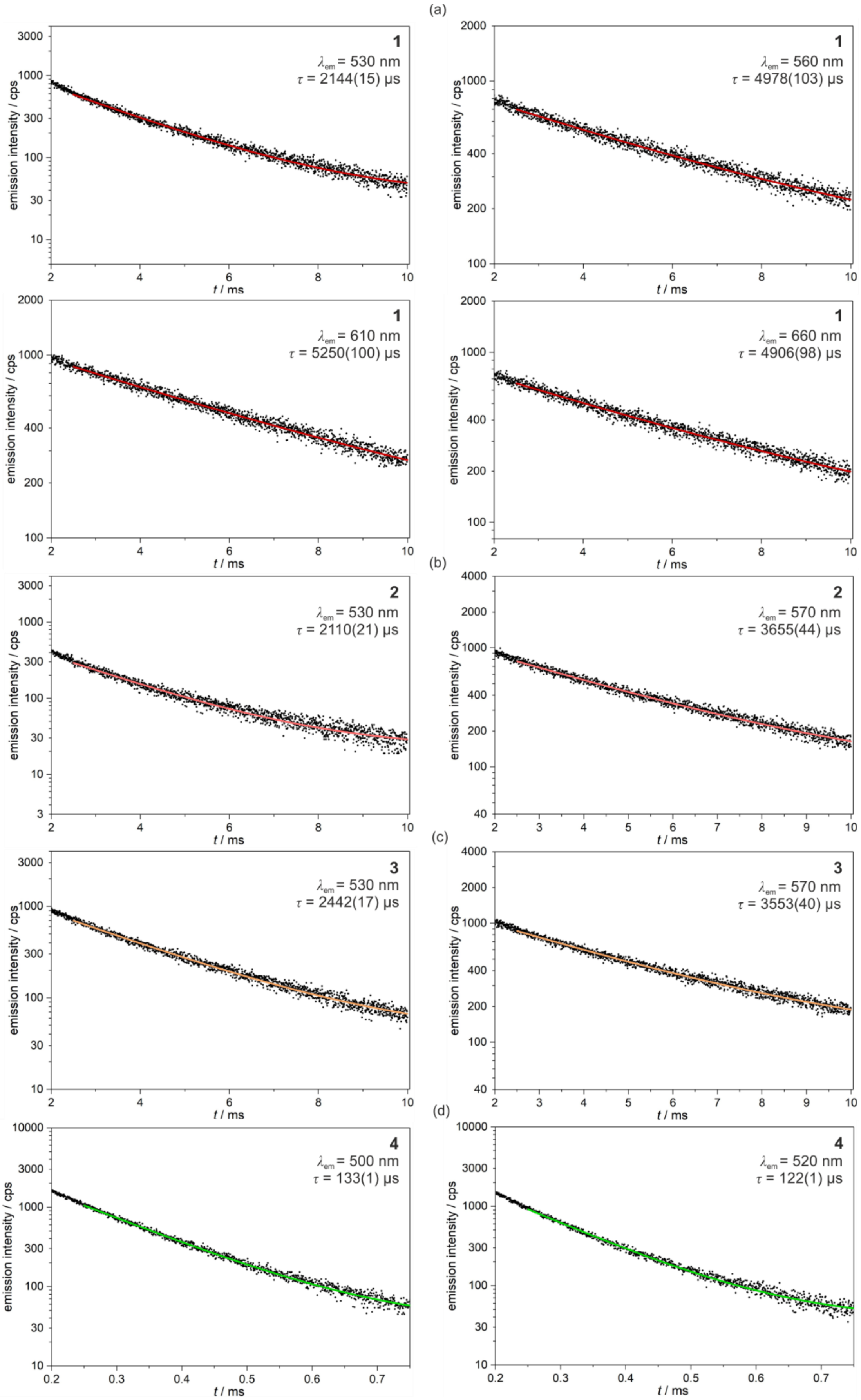

Figure S16. Representative emission decay profiles of **1** (*a*), **2** (*b*), **3** (*c*), and **4** (*d*) under λ_{exc} = 330 nm at indicated emission wavelengths. The black points show the experimental data while the coloured lines show the fitting using the mono-exponential decay function. The emission lifetimes are presented on the graphs and collected in Table S7.

Table S7. Parameters of the fittings of the emission decay profiles of **1**–**4** to the mono-exponential decay function.

compound **1**

emission wavelength with the assignment	emission lifetime at various excitation wavelength with the χ^2 parameters of the emission decay fitting			average lifetime for each emission wavelength
	λ_{exc} = 330 nm	380 nm	420 nm	
λ_{em}= 530 nm transition from S_{11}	τ = 2144(15) µs [χ^2 = 1.126]	2141(22) µs [1.045]	2183(28) µs [1.157]	**2156(22) µs**
560 nm transition from S_{10}	4978(103) µs [1.040]	5609(129) µs [1.039]	5419(117) µs [1.000]	5335(116) µs
610 nm transition from S_{10}	5250(100) µs [1.069]	5315(97) µs [1.051]	5361(104) µs [1.070]	5309(100) µs
660 nm transition from S_{10}	4906(98) µs [1.072]	4989(87) µs [1.125]	5314(102) µs [1.078]	5070(96) µs
average lifetime of the S_{10} state	5045(100) µs	5304(104) µs	5365(108) µs	**5238(104) µs**

compound **2**

emission wavelength with the assignment	emission lifetime at various excitation wavelength with the χ^2 parameters of the emission decay fitting				average lifetime for each emission wavelength
	290	330	380	420	
530 nm transition from S_{11}	too weak signal	2110(21) µs [1.044]	2204(31) µs [1.126]	2210(24) µs [1.119]	**2175(25) µs**
570 nm transition from S_{10}	3114(41) µs [1.121]	3655(44) µs [1.114]	3442(51) µs [1.073]	3367(34) µs [1.116]	3394(43) µs
610 nm transition from S_{10}	3475(41) µs [1.064]	3948(49) µs [1.065]	4028(59) µs [1.098]	3881(70) µs [1.023]	3833(55) µs
660 nm transition from S_{10}	3737(48) µs [1.007]	3906(65) µs [1.048]	4073(70) µs [1.077]	3887(56) µs [1.089]	3901(60) µs
average lifetime of the S_{10} state	3442(43) µs	3836(53) µs	3848(60) µs	3712(53) µs	**3709(53) µs**

compound **3**

emission wavelength with the assignment	emission lifetime at various excitation wavelength with the χ^2 parameters of the emission decay fitting				average lifetime for each emission wavelength
	260	330	380	420	
530 nm transition from S_{11}	2373(19) µs [1.127]	2442(17) µs [1.063]	2512(19) µs [1.097]	2514(18) µs [1.074]	**2460(18) µs**
570 nm transition from S_{10}	3518(43) µs [1.130]	3553(40) µs [1.042]	4020(58) µs [1.071]	3895(56) µs [1.046]	3747(49) µs
610 nm transition from S_{10}	3941(53) µs [1.048]	3901(55) µs [1.034]	4263(74) µs [1.054]	4486(82) µs [1.073]	4148(66) µs
660 nm transition from S_{10}	4214(61) µs [1.019]	4149(86) µs [1.106]	4389(91) µs [1.024]	4496(89) µs [1.075]	4312(82) µs
average lifetime of the S_{10} state	3891(52) µs	3868(60) µs	4224(74) µs	4292(76) µs	**4069(66) µs**

compound **4**

emission wavelength with the assignment	emission lifetime at various excitation wavelength with the χ^2 parameters of the emission decay fitting				average lifetime for each emission wavelength
	260	330	380	420	
500 nm $S_{10} \rightarrow S_{00}$ transition	142(1) µs [1.002]	133(1) µs [1.066]	126(1) µs [0.979]	124(1) µs [1.099]	131(1) µs
520 nm $S_{10} \rightarrow S_{01}$ transition	132(1) µs [1.110]	122(1) µs [1.055]	120(1) µs [1.094]	114(1) µs [1.116]	122(1) µs
average lifetime of the S_{10} state	137(1) µs	128(1) µs	123(1) µs	119(1) µs	**127(1) µs**

Table S8. Overview of the selected UO_2-based coordination networks or clusters revealing broad and/or red shifted uranyl charge transfer photoluminescence in comparison to the $UO_2(NO_3)_2\cdot 6H_2O$ salt.

compound	coordination dimensionality and coordination complex of U^{VI} centres	character of UO_2-based emission	position of the emission band, comparison with uranyl nitrate[S15] (λ_{max} = 510 nm)	proposed explanation of broad emission and its red shift	ref.
$(NH_4)_2[(UO_2)_6(O)_2(OH)_6(btca)]\cdot 6H_2O$ btca = pyromellitate anion	3D network based on $\{UO_2\}_3$ units three different $\{UO_7\}$ ions with oxo-O, hydroxo-O, and carboxyl-O	broad band in the 480–600 nm range	main maximum at 532 nm, red shift of 22 nm	role of the mixed oxo-/hydroxo-bridging	S16
$TMA_2[(UO_2)_2(bta)(H_2O)_2]\cdot H_2O$ TMA = trimethylammonium cation bta = 1,2,4,5-benzenetetracarboxylate	2D network based on $\{UO_2\}_4$ units two different uranyl complexes: $\{UO_7\}$ and $\{UO_8\}$ ions with carboxyl-O and bridging-aqua-O	broad band in the 500–590 nm range	main maximum at ca. 530 nm, red shift of ca. 20 nm	degeneration and overlap of the energy levels after coordination of bta ligand	S17
$X[(UO_2)_3(O)(OH)(H_2O)(1,2\text{-}bdc)_2]$ X = K^+, NH_4^+ 1,2-bdc = 1,2-benzenedicarboxylate	1D network based on $\{UO_2\}_2$ and $\{UO_2\}_4$ units three different uranyl complexes of $\{UO_7\}$ and $\{UO_8\}$ types with carboxyl-O, oxo-O, hydroxo-O, and aqua-O	broad band in the 490–600 nm range	main maximum at ca. 535 nm, red shift of ca. 25 nm	presence of oligomeric UO_2-based units leads to degeneration and overlap of energy levels	S18
$[(UO_2)(OH)(INT)]$ INT = isonicotinic anion	2D network with infinite hydroxo-bridged UO_2-based chain $\{UO_6N\}$ complexes with hydroxo-bridges	broad band in the 510–600 nm range	main maximum at ca. 540 nm, red shift of 30 nm	role of the uranium local coordination environment and the ligand effect *via* U-N bonding	S19
$(NH_4)_2[(UO_2)_6(O)_2(OH)_4(btec)_{1.5}]\cdot 11H_2O$ btca = pyromellitate anion	3D network based on $\{UO_2\}_3$ units three different $\{UO_7\}$ ions with oxo-O, hydroxo-O, and carboxyl-O	broad band in the 480–580 nm range	main maximum at ca. 530 nm, red shift of ca. 20 nm	role of the mixed oxo-/hydroxo-bridging	S20
$K_3[(UO_2)_{12}(O)_3(OH)_{13}(bdc)_4]\cdot 8H_2O$ bdc = 1,4-benzenetetracarboxylate	3D network based on $\{UO_2\}_3$ units three different $\{UO_7\}$ complexes with carboxyl-O, oxo-O, and hydroxo-O	broad band in the 490–600 nm range	main maximum at 535 nm, red shift of 25 nm	role of the mixed oxo-/hydroxo-bridging	S21
$[(UO_2)_3(O)(OH)_3(imdc)]\cdot 2H_2O$ imdc = 1,3-bis(carboxymethyl)-imidazolium	1D network of oxo-/hydroxo-bridged UO_2-based chains three different $\{UO_7\}$ complexes with carboxyl-O, oxo-O, and hydroxo-O	broad band in the 490–600 nm range	main maximum at 535 nm, red shift of 25 nm	role of the mixed oxo-/hydroxo-bridging	S22
$[UO_2(OCH(^iPr)_2)_2]_4$	0D tetranuclear cluster based on oxo-bridged UO_2 cations with additional alkoxide bridges four different $\{UO_6\}$ complexes with oxo-O and alkoxide-O atoms	broad band in the 540–660 nm range	main maximum at ca. 600 nm, red shift of ca. 80 nm	involvement of the oxo groups of UO_2 in the bridging to the next UO_2 units - strong change in the electronic structure of oxo ligands	S23

References to Table S8

[S15] A. F. Leung, L. Hayashibara and J. Spadaro, *J. Phys. Chem. Solids*, 1999, **60**, 299.

[S16] Y. Zhang, M. Bhadhade, I. Karatchevtseva, J. R. Price, H. Liu, Z. Zhang, L. Kong, J. Cejka, K. Lu and G. R. Lumpkin, *J. Solid State Chem*., 2015, **226**, 42.

[S17] Y.-N. Hou, Y.-H. Xing, F.-Y. Bai, Q.-L. Guan, X. Wang, R. Zhang and Z. Shi, *Spectrochim. Acta A*, 2014, **123**, 267.

[S18] I. Mihalcea, N. Henry and T. Loiseau, *Cryst. Growth Des*., 2011, **11**, 1940.

[S19] Y. Zhang, I. Karatchevtseva, J. R. Price, I. Aharonovich, F. Kadi, G. R. Lumpkin and F. Li, *RSC Adv*., 2015, **5**, 33249.

[S20] I. Mihalcea, N. Henry, C. Volkringer and T. Loiseau, *Cryst. Growth Des*., 2012, **12**, 526.

[S21] Y. Zhang, J. K. Clegg, K. Lu, G. R. Lumpkin, T. T. Tran, I. Aharonovich, N. Scales and F. Li, *ChemistrySelect*, 2016, **1**, 7.

[S22] N. P. Martin, C. Falaise, C. Volkringer, N. Henry, P. Farger, C. Falk, E. Delahaye, P. Rabu and T. Loiseau, *Inorg. Chem*., 2016, **55**, 8697.

[S23] M. P. Wilkerson, C. J. Burns, H. J. Dewey, J. M. Martin, D. E. Morris, R. T. Paine and B. L. Scott, *Inorg. Chem*., 2000, **39**, 5277.